STABILITY OF CRACKED CONCRETE HYDRAULIC STRUCTURES BY NONLINEAR QUASI-STATIC EXPLICIT FINITE ELEMENT AND 3D LIMIT EQUILIBRIUM METHODS

Flavien Vuillet[1], Mahdi Ben Ftima[2], Pierre Léger[3]

1-Graduate student, Department of Civil, Geological and Mining Engineering,
Polytechnique Montréal, Montreal University Campus, P.O. Box 6079, Station CV
Montréal, Québec, Canada, H3C 3A7
E-mail: flavien.vuillet@polymtl.ca

2-Assistant Professor, Department of Civil, Geological and Mining Engineering,
Polytechnique Montréal, Montreal University Campus, P.O. Box 6079, Station CV
Montréal, Québec, Canada, H3C 3A7
E-mail: mahdi.ben-ftima@polymtl.ca

3-Professor, Department of Civil, Geological and Mining Engineering,
Polytechnique Montréal, Montreal University Campus, P.O. Box 6079, Station CV
Montréal, Québec, Canada, H3C 3A7
E-mail: pierre.leger@polymtl.ca

Contact person:

Professor Mahdi Ben Ftima
Phone: (514) 340-4711 ext. 2298
Fax: (514) 340-5881
Email: mahdi.ben-ftima@polymtl.ca

Manuscript of a paper submitted for review and possible publication in
Computers & Structures

Revision 1: January 16, 2016

Abstract: Several hydraulic concrete structures suffer from severe tridimensional (3D) discrete cracking, producing an assembly of concrete blocks resting one on top of the other. It is important to consider the 3D particularities of the cracked surfaces in the nonlinear sliding safety evaluation of these structures. A methodology to assess a sliding safety factor (*SSF*) and a sliding direction ***D*** for any structure with an a priori known 3D discrete crack surface geometry using the quasi-static explicit nonlinear finite elements method (QSE-FEM) is presented herein in the context of the strength reduction approach. QSE-FEM is known for its efficiency in solving highly nonlinear problems compared to implicit FEM. However, in QSE-FEM, the determination of the incipient failure motion is challenging. In addition to the ratio of kinetic to internal strain energy, a new criterion is proposed to identify sliding initiation based on absolute displacements of a control point. As part of the proposed methodology, a complementary simple tool, 3D-LEM, has been developed as a 3D extension of the classical limit equilibrium method (LEM). It is useful in preliminary sliding analyses to estimate the critical friction coefficient inducing sliding and the corresponding direction ***D***. Three benchmark examples, of increasing complexities, are presented to verify the performance of the proposed methodology. Finally, a case study is adapted from an existing cracked hydraulic structure to evaluate its sliding stability using the QSE-FEM and 3D-LEM approaches. In the three benchmark examples, the same results are found for *SSF* and ***D*** for the two approaches. In the hydraulic structure example, SSF_{LEM}, computed with 3D-LEM, is a lower bound of SSF_{FEM} from QSE-FEM, and a strong correlation is found between the sliding directions computed with the two approaches.

Keywords: Finite elements; quasi-static explicit analyses; limit equilibrium; three-dimensional analyses; sliding safety assessment, concrete hydraulic structure

1 Introduction

Several concrete gravity dams and spillways have been subjected to severe three-dimensional (3D) discrete cracks induced, for example, by concrete expansion due to alkali aggregate reaction (AAR), producing an assembly of unreinforced cracked mass concrete blocks resting one on top of the other (Fig. 1). Discrete cracks of complex non-planar and irregular surface geometries tend to occur and become localised in structures exhibiting geometrical and stiffness discontinuities along their longitudinal axes. As typical examples, the following structures showing this type of damage pattern have been reported in the literature: Beauharnois dam, Canada [1]; Fontana dam, USA [2]; La Tuque dam, Canada [3]; Chambon dam, France [4] and Temple-sur-Lot spillway piers [5, 6]. The definition of the crack surface topology (Figs. 1b and 1c) is possible through site investigation using: (i) visual inspection of crack contour on the downstream face and the exposed pier surfaces; (ii) inspection with a geo-camera installed on a submarine for the upstream face, and (iii) concrete vertical drilling from the dam crest. For this type of cracked concrete hydraulic structure, it is important to consider the 3D particularities of the crack contacting surface geometries in the presence of uplift pressures. The finite element (FE) solution to detect 3D relative crack surface motions of arbitrary geometry, leading to sliding or rotational failure mechanisms, is a highly nonlinear frictional contact problem that is difficult to solve using the classical nonlinear implicit finite element method (FEM). For sliding stability, FEM using a Mohr-Coulomb frictional model can be performed using the strength reduction method in which the friction coefficient is progressively reduced to induce sliding displacements. Strength reduction method has been successively applied in the field of geotechnical engineering for quantifying slope stability. Recently, Tu et al. [7] used FLAC3D to study the stability of 2D and 3D slope problems. Energy based criteria were developed to define the incipient slope failure. The criteria are based on

85 detecting changes in kinetic, potential or strain energy of the model. The results were consistent
86 with the safety factors determined by conventional criteria based on changes in the stresses, strain
87 or displacement distributions in the slope. Though the results were satisfying using the energy
88 criteria, they were applied on simpler problems, if compared to the case study problem shown in
89 Fig. 1. The applicability of Tu et al. [7] methodology based on energy criteria is therefore
90 questionable for the general case where the geometry of the failure surface is arbitrary and where
91 the direction of the sliding is not easily predictable.
92 Constitutive laws for materials can also exhibit highly nonlinear softening behaviour due to alkali–
93 aggregate reaction (AAR) degradation or other structural effects. Convergence difficulties may
94 arise when using the conventional implicit FEM in the context of large concrete models, leading
95 to premature "numerical" failure [8]. Using the explicit FEM approach, the numerical problem is
96 solved dynamically using Newton's second law of motion. This approach was found to be very
97 efficient for solving highly nonlinear problems such as impact and large displacement problems
98 [9]. The distinct element method (DEM), using an explicit solution algorithm, has been widely
99 used for stability assessment of jointed rock slopes, tunnels and dam foundations [10]. DEM
100 commercial software such as UDEC/3DEC recognize individual discontinuities by modelling
101 joints using appropriate distinct (discontinuous) constitutive models from models used for the bulk
102 material. This is in opposition to the classical continuum FEM where the presence of
103 discontinuities in the bulk material has to be represented indirectly in the average sense (i.e.
104 smeared crack models). Lisjack and Grasseli [11] presented a comprehensive review of DEM
105 techniques to assess fracturing of rock masses. Recently, Zhou et al. [12] used ABAQUS/Explicit
106 to develop a combined finite-discrete element method. In their work, a rock mass is idealised as
107 numerous elastic block elements interacting through cohesive joints modeled as contact elements

located along their boundaries. Geomechanical problems have been solved at scales ranging from concrete cylinders to slope stability using thousand of discrete elements. The limit equilibrium was reached by increasing the gravitational "constant" (element self-weight) until sliding is detected. The velocity field and the total kinetic energy were used as slope stability indicators. Lately, Abaqus/Explicit models have been applied in the field of concrete hydraulic structures using the quasi-static approach [13, 14]. The nonlinear quasi-static explicit finite element method (QSE-FEM) is used in this work as an alternative to the classical implicit FEM. QSE-FEM requires the definition and interpretation of criteria to detect the loss of static equilibrium leading to instability with respect to the initial position. In addition to the kinetic energy criterion used in the previous studies [8, 12, 13, 14], one additional criterion is proposed herein: the absolute crack surface motions at particular degrees of freedom (DOF). In addition, simple tools, such as the classical limit equilibrium method, should be used for verification purposes to bound the sliding safety factors computed from QSE-FEM. For that purpose, a 3D extension of the 2D limit equilibrium method [15], labelled as 3D-LEM, has been developed and implemented in a MATLAB® code as a complementary tool to QSE-FEM. 3D-LEM uses a directional search algorithm to find the minimum sliding safety factor (SSF_{LEM}) and related sliding direction. 3D-LEM is found to be a lower bound solution compared to QSE-FEM. The proposed solution strategies are general and could be applied to any concrete structure with discrete cracks.

This paper is organised as follows. First, the QSE-FEM tool is presented. The 3D extension of the classical 2D limit equilibrium algorithm, 3D-LEM, is then developed. An analysis methodology is proposed using QSE-FEM and 3D-LEM as complementary tools. Three validation examples of increasing complexity are investigated to illustrate the particularities of the 3D stability problem. Finally, a case study, adapted from an actual cracked hydraulic structure, as shown in Fig. 1, is

analysed showing the performance of QSE-FEM and 3D-LEM. Though applied on an example of hydraulic structure, the framework developed in this study can be applied to a wider range of civil engineering problems where failure may occur through complex and arbitrary 3D surface.

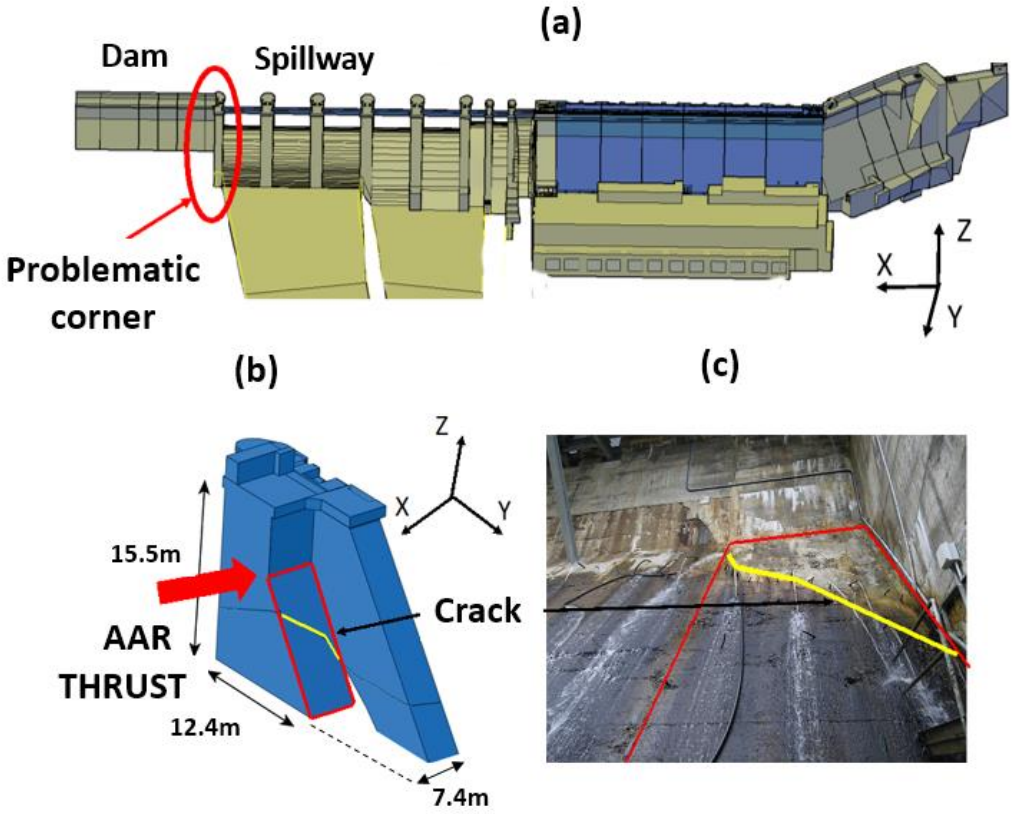

Figure 1: 3D discrete cracking due to AAR expansion: (a) 3D view of hydraulic facility; (b) problematic corner showing 3D discrete cracking; (c) crack mapping on existing structure

2. Nonlinear quasi-static explicit FEM

The explicit dynamics approach was developed and successfully applied in the industrial field of metal forming at the beginning of the nineties [16]. The explicit approach was implemented in several commercial packages (e.g., ABAQUS-Explicit in ABAQUS [9], LS-DYNA [17]).

Following an explicit formulation, the nonlinear problem is solved using dynamic equilibrium equations. Conventional nodal forces are converted into inertia forces by assigning lumped masses to nodal DOFs. The dynamic equilibrium equations are written in terms of inertia forces, where $\boldsymbol{M}$ is the lumped mass matrix of the model, $\boldsymbol{P}$ is the external load vector, and $\boldsymbol{I}$ is the internal load vector:

$$\boldsymbol{M\ddot{u} = P - I} \quad (1)$$

Compared to the conventional implicit approach, no iteration is performed. The transient solution algorithm advances explicitly in time using a very small time increment to ensure stability. This increment, Δt, depends on the smallest element of the mesh and can be as low as 10^{-5} to 10^{-7} fraction of the total analysis time, t_{exp} (Fig. 2). The original nonlinear static problem is solved in a quasi-static manner when the first term in Eq. (1) is negligible. This can be accomplished by applying the loads "slowly enough" with respect to the fundamental period of vibration, T_1, to ensure that kinetic energy, E_k, is negligible compared to the internal strain energy, E_i, [8,9]. As shown in Fig. 2a, a smooth loading time, t_L, is suggested for each load applied separately, such as self-weight, hydrostatic thrusts and uplift pressures, using an established rule of thumb of 20 T_1 to 50 T_1 for the loading time t_L [8]. This ensures an acceptable evolution of the energy ratio E_k/E_i over time as shown in Fig. 2b. Each peak $(t_i, r_i), i > 1$, in Fig. 2b represents a typical nonlinear "major event" (e.g., macro-crack propagation in a reinforced concrete beam or local sliding of a surface in a Mohr-Coulomb stability problem). Two important *quasi-static criteria* must be met for the energy response: (1) considering an energetic criterion, $C_{Eng} = E_k/E_i$, the magnitude of C_{Eng} at the peaks i for $i > 1$ should be less than 5% ($C_{Eng} \leq 5\%$); (2) the behaviour of the model shall remain linear elastic within the initial "acceleration" period between 0 and t_0 (Fig. 2b) to

avoid a sudden (dynamic) release of stored elastic energy due to damage. By respecting these two quasi-static criteria, the failure time t_f of the model is defined as the time where C_{Eng} *irreversibly* exceeds a threshold value (e.g., $C_{Eng} > 5\%$).

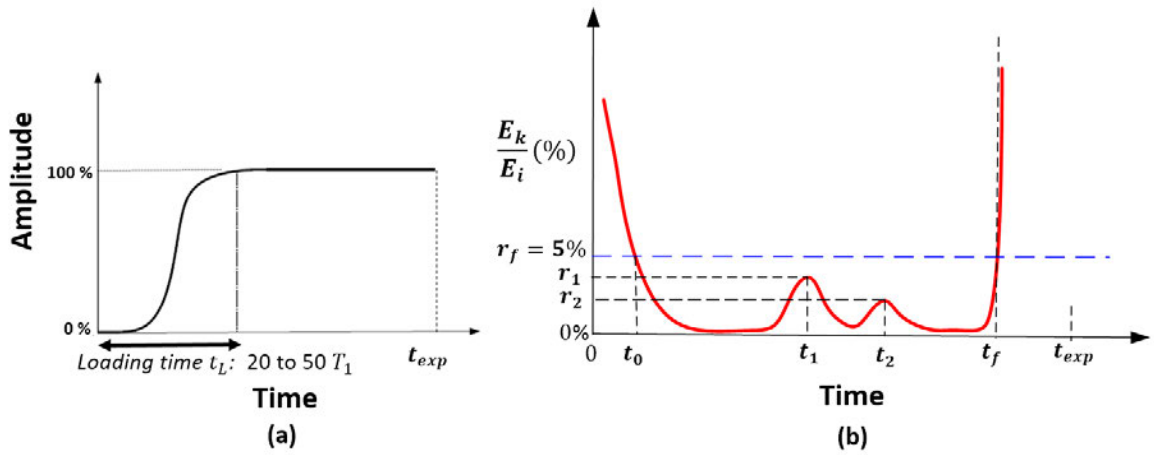

Figure 2: QSE-FEM: (a) loading smooth amplitude; (b) typical curve for energy ratio versus time

In this work, the ABAQUS-Explicit framework is used within the commercial package ABAQUS [9]. The *General contact* algorithm available in ABAQUS-Explicit is used. It is a robust automatic contact algorithm able to solve complicated and very general 3D contact problems. This contact algorithm has been used extensively in the industry to solve impact tests and automobile crash tests [18]. Using a sophisticated tracking algorithm over the contact domain, the software identifies all node-to-face and edge-to-edge penetrations at each explicit time increment and uses a penalty enforcement of contact constraint in the normal direction. A large displacement sliding method is used in tangential directions, which allows for arbitrary separation, sliding and rotation of surfaces in contact. In the tangential (sliding) direction, displacement continuity is exactly enforced during the stick condition. The sliding constitutive model in the tangential direction neglects the related crack dilation motions in the normal direction due to the interface crack roughness. The dilation

effect of concrete-concrete sliding interfaces is implicitly considered in the selected initial friction coefficient according to test data [19] and dam safety guidelines. For the strength reduction method used in this study, a user subroutine, called *VFRIC,* was programmed to model a user-defined tangential strength, which allows for a progressive decrease in the friction coefficient over time $\mu i(t)$. The typical variation of $\mu i(t)$ is shown in Fig. 3a. The t_j and $\mu i(t_j)$ values are user inputs to the subroutine required to compute a continuous curve with smooth interpolation (cubic polynomial) between successive time points. The Mohr-Coulomb criterion is used for sliding with zero cohesion. All computations are performed with static friction coefficients in contrast to using static and dynamic friction coefficients. The first value μi_0 is the initial value of the friction coefficient, constant for the first loading step, which is a local material property for the **"ith"** discretized FE contact surface. Of course, these friction coefficients must be larger than the critical friction coefficient value that induce sliding.

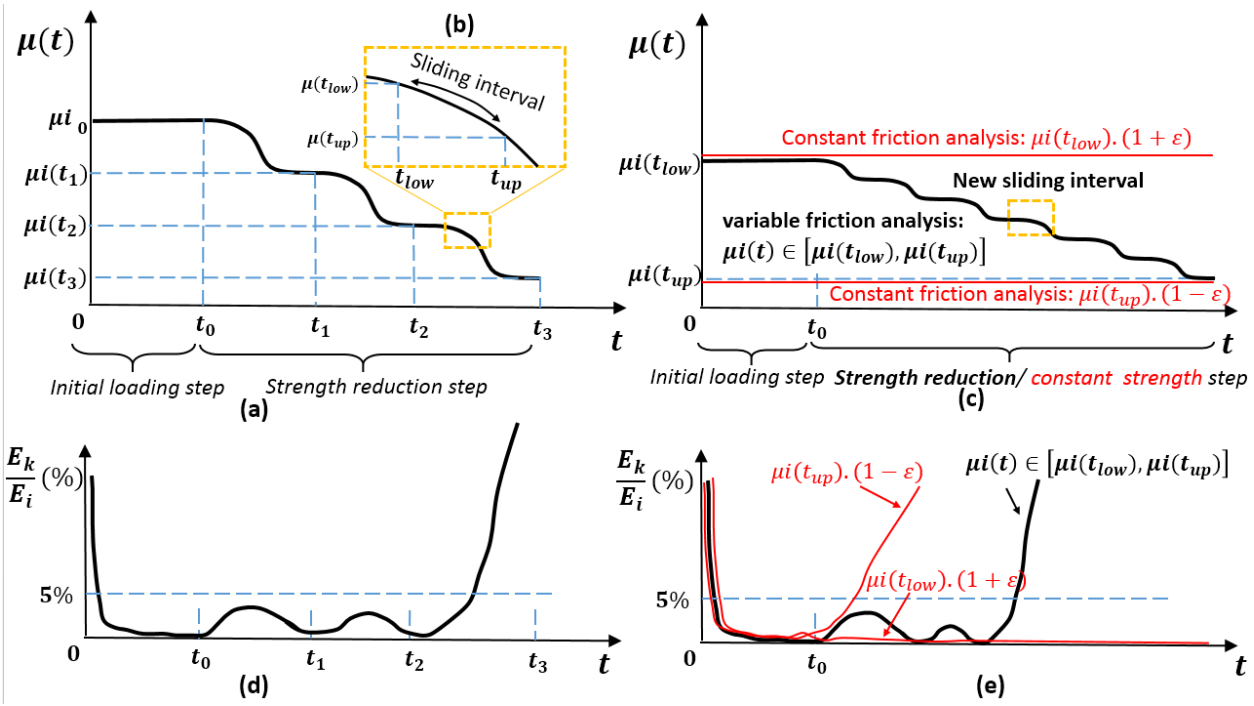

Figure 3: Procedure used in strength reduction method: (a) variable friction in the *tracking phase*; (b) sliding interval tracking; (c) constant friction and variable friction analyses in the *verification/refinement phases* (regular/bold lines); (d) energy ratio evolution in the *tracking phase*; (e) energy ratio evolution in the *verification/refinement phases* (regular/bold lines)

In addition to the energy criterion, C_{Eng}, a displacement criterion, C_{Disp}, is defined herein. C_{Disp} is related to the absolute displacement magnitude of a selected *control point* from the upper sliding block. Due to the relatively large magnitude of the sliding displacement with respect to the elastic displacement induced by the deformations of the upper and lower blocks and to the large sliding velocity that is initiated by a sliding failure, it was found that using the absolute displacement is precise enough to detect the onset of the instability (sliding) phase. The *control point* is a point

belonging to the upper sliding surface. It is located at the extremity of the last resisting elements with respect to the sliding direction, ***D***. An example of a control point is presented in the third example of section 5 (Fig. 9). In a more general 3D problem, the selection of the control point and sliding direction is not easily predictable. 3D-LEM is thus introduced in section 3 as a preliminary predictive tool to complement the QSE-FEM analysis. The strength reduction factor *SRF(t)* is introduced as the ratio between initial and reduced friction coefficients: $SRF(t) = \mu i_0 / \mu i(t)$ (Fig. 3a). Using the C_{Eng} and C_{Disp} criteria, the *SRF* that induces sliding is identified. SSF_{FEM} is defined as the last value of *SRF* where a stable condition is maintained.

3 3D Extension of limit equilibrium method

3.1 2D limit equilibrium method

The bi-dimensional limit equilibrium method (2D-LEM) was documented by the US Army Corps of Engineers in 1981 [20]. The method defines SSF_{LEM}:

$$SSF_{LEM} = \frac{\tau_a}{\tau} \quad (2)$$

where τ_a is the admissible shear stress, and τ is the shear stress on the failure plane. The admissible shear stress is ruled by the Mohr–Coulomb equation:

$$\tau_a = c + \sigma * \tan(\phi) \quad (3)$$

where c is the cohesion, σ is the normal pressure to the failure plane, and ϕ is the friction angle.

SSF_{LEM} in Eq. (2) can be applied only on a single wedge with a straight cracked plane. An algorithm was thus developed to solve the multi-wedge problem associated with a segmented cracked surface (Fig. 4a). Each segment of the cracked surface defines a wedge by vertical delimitation to each extremity of the segment. Horizontal thrusts, $\boldsymbol{P_{i-1}}$ and $\boldsymbol{P_i}$, are introduced on the left and right sides

of each wedge to equilibrate the shear stress on its bottom segment (Fig. 4b). The force difference, $\boldsymbol{P_{i-1} - P_i}$, is computed as follows:

$$\boldsymbol{P_{i-1} - P_i} = \frac{((\boldsymbol{W_i}+\boldsymbol{V_i})*\cos(\alpha_i) - \boldsymbol{U_i})\frac{\tan(\phi_i)}{SSF_{LEM}} - (\boldsymbol{W_i}+\boldsymbol{V_i})*\sin(\alpha_i) + \frac{c_i}{SSF_{LEM}}*L_i}{\cos(\alpha_i)+\sin(\alpha_i)*\frac{\tan(\phi_i)}{SSF_{LEM}}} \quad (4)$$

where $\boldsymbol{W_i}$ is the weight of the wedge, $\boldsymbol{V_i}$ is the weight of the water above, $\boldsymbol{U_i}$ is the uplift**,** $\boldsymbol{L_i}$ is the length of the $\mathbf{i}^{th}$ segment, and $\boldsymbol{\alpha_i}$ is the angle between this segment and the horizontal. The SSF_{LEM} corresponding to the sliding limit equilibrium is computed such that the summation of all $\boldsymbol{P_{i-1} - P_i}$ is nearly zero. Moment equilibrium is not satisfied. Therefore, only a global equilibrium of driving versus resisting sliding forces is satisfied along a unique kinematic admissible sliding direction, $\boldsymbol{D}$, which is horizontal for the case in Fig. 4.

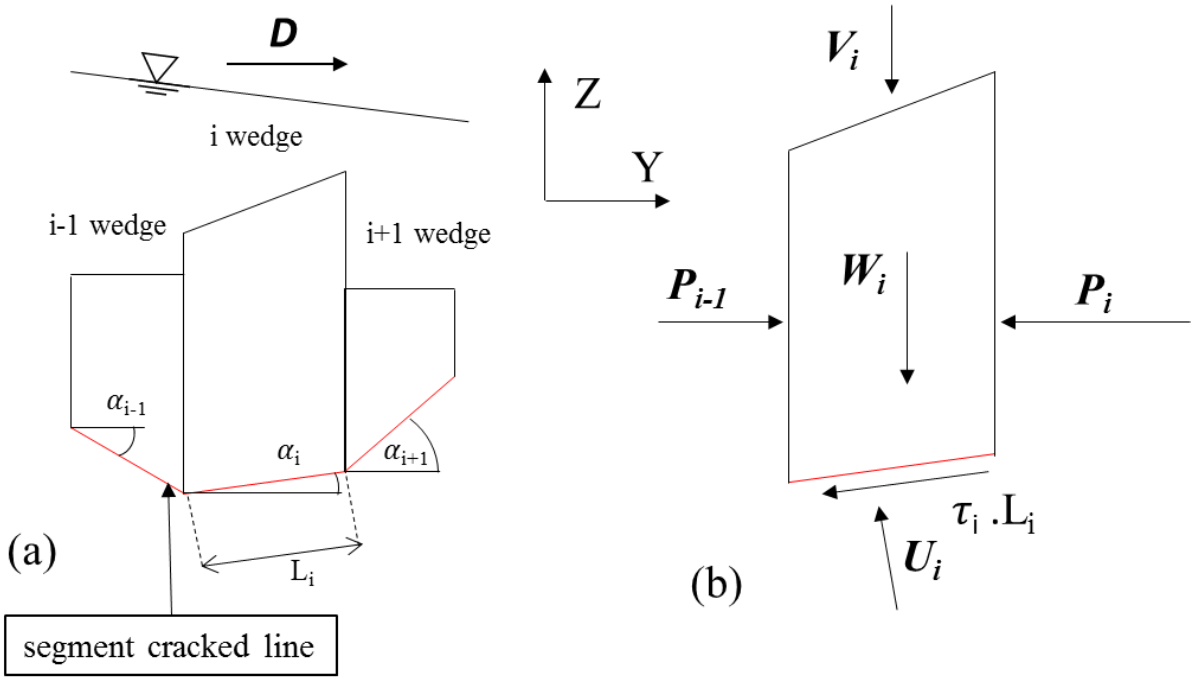

Figure 4: 2D limit equilibrium method; (a) three wedges example; (b) loads on a single wedge

239

240 **3.2 3D extension of limit equilibrium method**

241 The 3D limit equilibrium method (3D-LEM) is defined as an extension of the classical 2D-LEM
242 presented in section 3.1. Fig. 5a presents part of a gravity dam (or an arbitrary concrete structure)
243 with a nonplanar crack pattern at its base. The complete cracked surface is discretized by several
244 elementary triangular surfaces. The volume of the complete structure is divided into adjacent
245 vertical elementary elements labelled as "columns" located between a particular triangle at the
246 cracked surface and the top of the structure. Each column denoted by the index "i", and its related
247 base triangular surface described by nodes 1-2-3, is subjected to several forces: the self-weight,
248 $\boldsymbol{W_i}$, the uplift pressures, $\boldsymbol{U_i}$, an arbitrary resultant of external forces, $\boldsymbol{F_i}$, and the forces $\boldsymbol{P_i}$ and $\boldsymbol{P_{i-1}}$
249 associated with the LEM, which equilibrate the shear strain on the base of the column (Fig. 5b).
250 The self-weight of a column, $\boldsymbol{W_i}$, is defined by the product of material density and the column
251 volume computed from the known geometry. Water pressures are associated with each corner of
252 the base triangle. The average value defines the elementary uplift pressure that is multiplied by the
253 base triangular surface to obtain the uplift force, $\boldsymbol{U_i}$. The external thrust $\boldsymbol{F_i}$, could be null or could
254 be the resultant of hydrostatic pressure as an example.

255

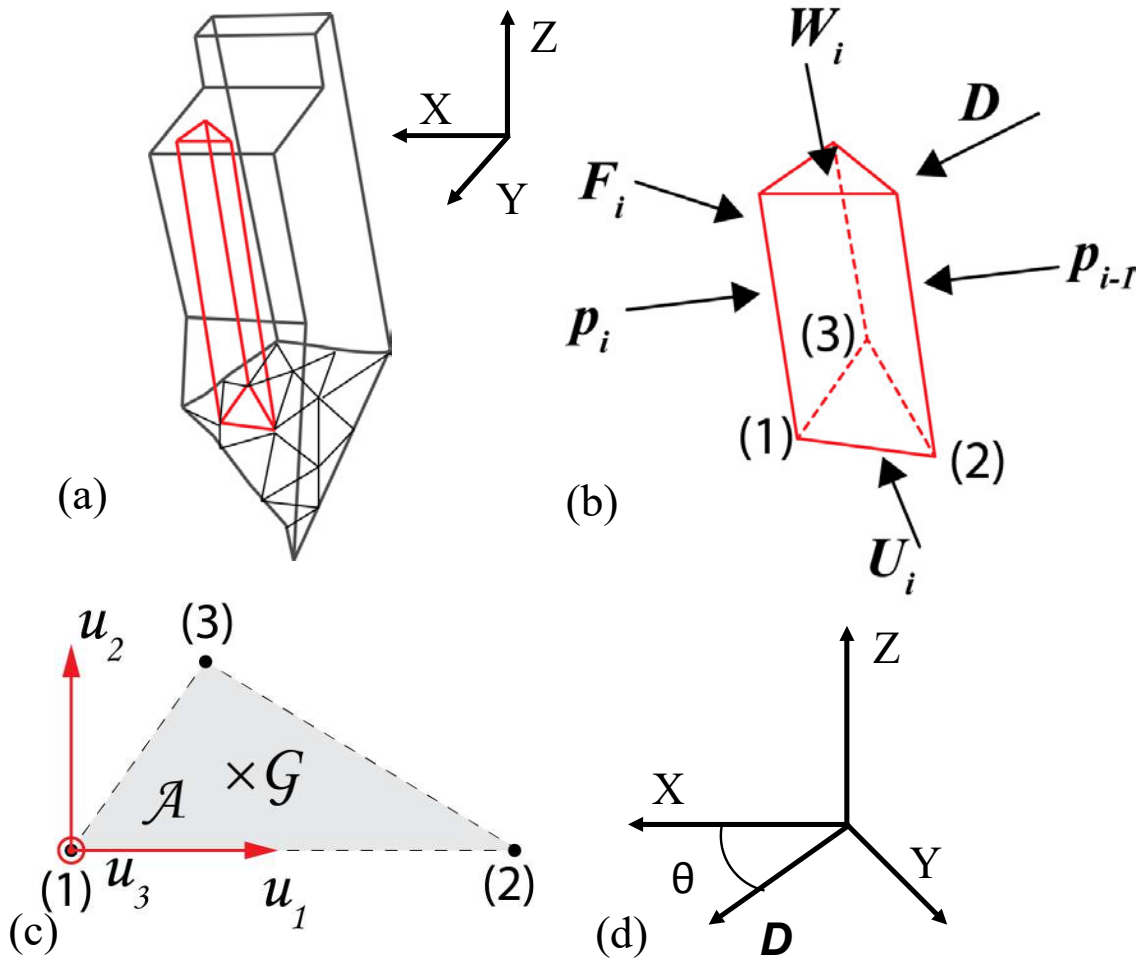

256

257 Figure 5: Definition of 3D-LEM (a) cracked surface divided into triangles and concrete block
258 divided into columns; (b) loads applied on a column; (c) local axis definition for the triangular
259 base; (d) definition of θ and the sliding direction $\boldsymbol{D}$

260

261 The elementary unbalanced horizontal forces, $\boldsymbol{P_{i-1} - P_i}$ or $\boldsymbol{\Delta P}$, are to be computed for each
262 column, following a given direction $\boldsymbol{D}$. The limit equilibrium condition of the surface along the
263 direction $\boldsymbol{D}$ gives the following equation:

$$\frac{c * A}{SSF} - (\boldsymbol{W + U + F + \Delta P}).\boldsymbol{u_3} * \frac{\tan(\Phi)}{SSF} = (\boldsymbol{F + W + \Delta P}).\frac{\boldsymbol{D'}}{||\boldsymbol{D'}||} \qquad (5)$$

where

$$\boldsymbol{D'} = \boldsymbol{D} - (\boldsymbol{u_3}.\boldsymbol{D})\boldsymbol{u_3} \quad (6)$$

$(\boldsymbol{u_1}\ \boldsymbol{u_2}\ \boldsymbol{u_3})$ defines a local axis system linked to the triangular column base (Fig. 5c). The parameter $\boldsymbol{u_1}$ is a normalised vector from node 1 to node 2 of the triangle, and $\boldsymbol{u_3}$ is normal to the triangle and oriented such that the scalar product $\boldsymbol{u_3}.\boldsymbol{Z} \geq \boldsymbol{0}$. The vector $\boldsymbol{u_2} = \boldsymbol{u_3}\hat{}\boldsymbol{u_1}$ is complementary and located in the plane of the triangle. The interface properties introduced in Eqs. (2) and (3) for failure planes in the conventional 2D-LEM are assumed constant for each triangular element at the interface cracked surface and are defined as local material properties for the "$\mathbf{i^{th}}$" discretized FE contact surface. The Mohr-Coulomb equation rules the contact between surfaces, such that a friction coefficient, $\mu i_{crack} = \tan(\Phi)$ and a cohesion, c_i, are associated with the "i^{th}" contact surface.

$\boldsymbol{P_{i-1}} - \boldsymbol{P_i}$ is defined along this same direction $\boldsymbol{D}$:

$$\boldsymbol{\Delta P} = \boldsymbol{P_i} - \boldsymbol{P_{i-1}} = P * \boldsymbol{D} \quad (7)$$

The direction $\boldsymbol{D}$ is horizontal and is defined by the angle θ (Fig. 5d). It is assumed that the strength is developed in direction $\boldsymbol{D}$ such that the resisting forces associated with the cohesion and the friction are also along this direction. A vector $\boldsymbol{\Delta P}$ is computed for each column.

Similar to the 2D-LEM method, the *SSF(**D**)* is determined when $\sum_i \boldsymbol{\Delta P}_i = 0$. Newton's method is used to find the "zero" of the summation, which has the advantages of simplicity and quadratic convergence. *SSF*($\boldsymbol{D}$) is computed for each direction $\boldsymbol{D}$, and the minimum is identified as SSF_{LEM} related to the corresponding sliding direction, $\boldsymbol{D_{LEM}}$.

The convergence tolerance to satisfy the equation $\sum_i \boldsymbol{\Delta P}_i \cong 0$ has a strong influence on the SSF_{LEM} results. Fig. 6 illustrates several curves drawn for different tolerances where $\sum_i \boldsymbol{\Delta P}_i = 10^{-1}$ to 10^{-4}. A "small" tolerance is required for smooth response curves. A real improvement occurs for tolerances smaller than or equal than 10^{-3}; a 10^{-3} tolerance value is thus used later in the application examples.

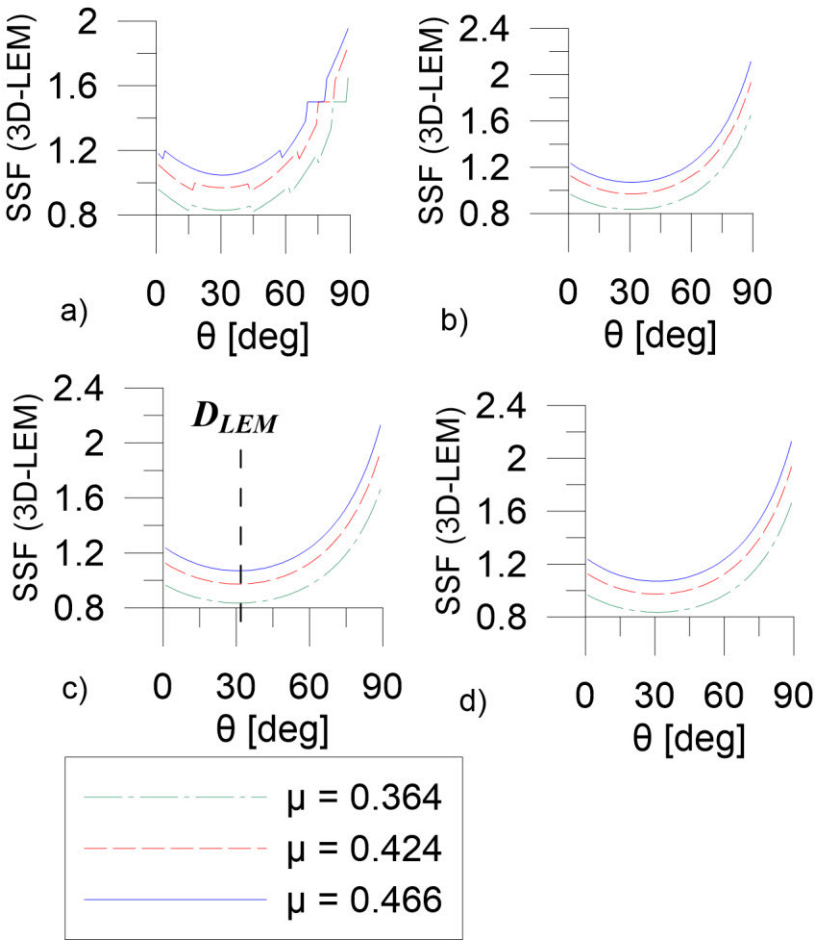

Figure 6: Influence of the tolerance on *SSF(**D**)* (example 2 considered); (a) tolerance=10^{-1}; (b) tolerance=10^{-2}; (c) tolerance=10^{-3}, $\boldsymbol{D}_{LEM}=\boldsymbol{D}$ (θ=30.67deg); (d) tolerance=10^{-4}

Eq. (4) could become ill conditioned if the denominator is close to zero. Ebeling et al. [15] suggested that the denominator in Eq. (4) should not be less than 0.2. In 3D-LEM, the ill condition problem is solved by slightly modifying the inclination of the base triangle of problematic columns. The inclination is reduced so that the normal to the base becomes closer to the vertical axis Z. This operation locally modifies the geometry of the cracked surface, but it is acceptable in practice for a structure such as that shown in Fig. 1 because uncertainty always remains on the exact geometry of the crack surfaces.

4 Proposed methodology for sliding safety assessment

A progressive assessment methodology is suggested in this work, based on the experienced gained through the several numerical studies conducted. 3D-LEM is found to be a simple tool compared to QSE-FEM, giving a lower bound value of SSF_{FEM}. QSE-FEM is a sophisticated FE tool that considers all types of potential unstable conditions by computation of the incipient kinematic motions of all cracked components in the model. It is therefore relevant to any general 3D stability problem: rigid/deformable bodies, linear/nonlinear constitutive material, small/large displacements, imposed displacements/forces, sliding/overturning/uplifting or any combination of these relative motions. As with any sophisticated tool, using QSE-FEM represents challenges in terms of *problem sensitivity* and *abundance* of results. The analysis should thus be performed as follows:

a) *Discretization of the geometry:* discretization into triangles of the 3D discrete cracked surfaces in 3D-LEM and 3D discretization with solid elements in the FE model used in QSE-FEM. For consistency, the discrete cracked surfaces are generated with ABAQUS and used as input to MATLAB®.

b) *Selection of time integration parameters*: Compute the stable time increment Δt for the QSE-FEM generated mesh. Compute the modal frequencies of the FE model by imposing the full compatibility condition in the interfaces between all cracked components (or wedges) of the model (TIED condition) and fixity condition at the bottom face of the foundation block. Define accordingly t_{exp} for the analysis duration and t_L for each load condition. Proceed with preliminary analyses using QSE-FEM (only with an initial loading step, t_L) to check the quasi-static criteria.

c) *Directional search:* Proceed with a directional search with 3D-LEM to find SSF_{LEM} and $\boldsymbol{D_{LEM}}$.

d) *Initialisation of QSE-FEM*: Use the results of step c) to select an initial value of the friction coefficient μi_0 and a control point to monitor the onset of the sliding (criterion C_{Disp}).

e) *Perform strength reduction:* Move forward with a strength reduction step in QSE-FEM within a first tracking phase (Figs 3a, b and d). Identify a sliding interval range using a lower bound and an upper bound, $\left[\mu i(t_{low}), \mu i(t_{up})\right]$, for μi_{crit} (criteria C_{Eng} and C_{Disp} are considered; only C_{Eng} is shown in Fig. 3d).

f) *Verification and refinement to compute μi_{crit}*: In this step, three different analyses are considered as shown in Fig. 3c. For verification of the sliding interval range, two analyses with constant friction coefficients are conducted. The values of the friction coefficients are selected to be slightly outside the sliding interval range (an ε value of 0.05 to 0.1 is to be used). It may happen that, contrary to what is shown in Fig. 3e, the criterion C_{Eng} for the case $\mu i(t_{up}).(1-\epsilon)$ decreases after t_0 and follows a tendency similar to the case $\mu i(t_{low}).(1+\epsilon)$. The reason for this behaviour is the presence of residual inertia forces for each smooth step delimited by t_j and t_{j+1}. This behaviour is schematically shown in

Fig. 3d at the end of the interval $[t_0, t_1]$. It is necessary for this particular case to return to the tracking phase and set up new bounds of the sliding interval. The increase in the interval length (e.g., the interval $[t_0, t_1]$ for the case depicted in Fig. 3) was found to be an efficient solution to reduce the magnitude of the inertia forces. The next step is the refinement of the μi_{crit} interval range. An analysis with a variable friction coefficient is therefore used (Figs. 3c and e). Similar to the tracking phase, a first initial loading step with constant friction coefficient $\mu i(t_{low})$ is followed by a strength reduction step with friction coefficient smoothly decreasing from $\mu i(t_{low})$ to $\mu i(t_{up})$ (Figs. 3c and e).

g) *Computation of SSF_{FEM}*: Estimate the value of the critical friction coefficient, μi_{crit}, the corresponding $SSF_{FEM} = \frac{\mu i_{crack}}{\mu i_{crit}}$ and the corresponding sliding direction, $\boldsymbol{D_{FEM}}$.

Complementary analyses could be performed in step f) *Verification and refinement to compute μi_{crit}* using implicit FEM on the two analyses with constant friction coefficients. If both analyses with constant friction coefficients $\mu i(t_{low})$ and $\mu i(t_{up})$ converge, the interval range $[\mu i(t_{low}), \mu i(t_{up})]$ is incorrect. The analysis using the coefficient value $\mu i(t_{up})$ should not lead to an equilibrium state. The methodology then must be initiated again in step e). In any other case, one analysis or both analyses fail such that no conclusion can be deduced due to the possibility of a "numerical" failure of the implicit analyses.

5 Validation examples

Three validation examples are considered in this section. They represent important issues related to the real case study problem introduced in Fig. 1b. Sliding on an arbitrary inclined plane and tracking of the critical sliding direction are considered in example 1. The problem of locally large uplift pressure with respect to gravity loads, which may occur in the downstream inclined face of a dam (Fig. 1b), is considered in example 2. The multiple-wedge issue is considered in example 3,

362 taken from [20]. In addition to [20], example 1 and example 2 can be considered as new benchmark
363 *unit problems* that can be used for the *verification and validation* purposes (*V&V*) of the stability
364 assessment tool of a general 3D problem.

365 • *Example 1 – 3D sliding block on an inclined surface*

366 This first example illustrates a 3D stability problem of a single massless block sliding on an
367 arbitrary inclined surface (Fig. 7a). Two external driving forces are applied, 5 kN along the Z-axis
368 and 1 kN along the X-axis (Fig. 7b). A sliding analysis direction is required to compute SSF_{LEM}.
369 This direction is projected in the XY plane and is characterized by a directional angle θ defined
370 from the X-axis (Fig. 7d). Sets of $SSF(\boldsymbol{D}(\theta))$ results are computed for series friction coefficients,
371 μ, and for a range of θ (Fig. 7c). The curve tangent to a $SSF(\boldsymbol{D})$ = 1 defines the minimal friction
372 coefficient for limit equilibrium, which is equal to μ_{LEM} = 0.435. $SSF(\boldsymbol{D})$ increases with increasing
373 friction coefficient μ regardless of the potential sliding direction $\boldsymbol{D}$. Minimum $SSF(\boldsymbol{D})$, SFF_{LEM}, is
374 always reached at the directional angle θ_{LEM} = 30.67°, irrespective of the friction coefficient. The
375 red point in Fig. 7c indicates $\mu_{FEM} = 0.437$ computed using QSE-FEM. The sliding motion
376 projected in the XY plane is shown in Fig. 7d. It is a rectilinear motion with a 29.33° directional
377 angle between the X-axis and the sliding direction. $\mu_{FEM} = 0.437$ develops the frictional strength
378 just able to maintain equilibrium (incipient sliding motion), which has less than 1% difference with
379 μ_{LEM}. These nearly identical results between μ_{LEM} and μ_{FEM} validate the two stability analysis
380 tools used to characterize the limit friction coefficient and the incipient sliding direction for this
381 basic 3D sliding problem.

382

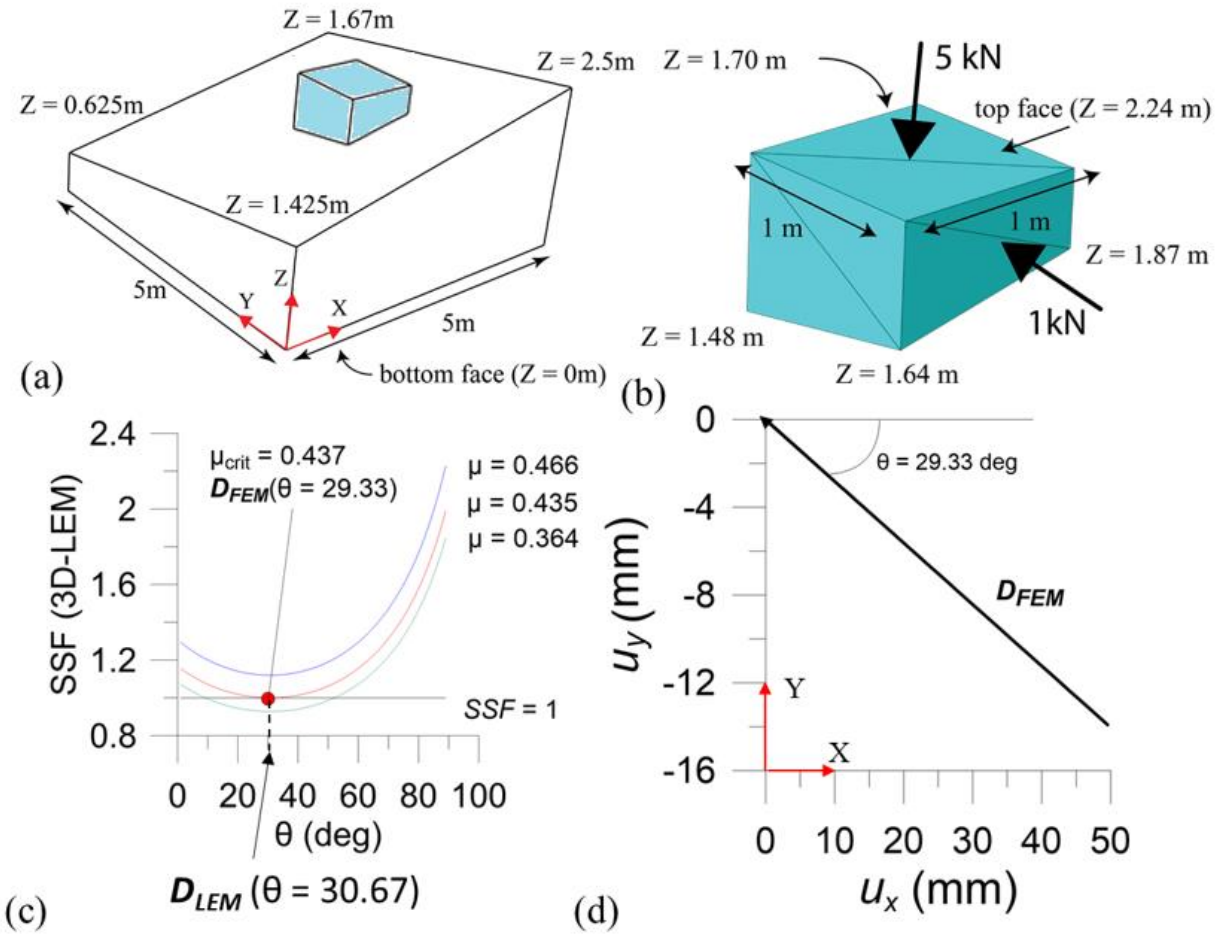

Figure 7: Example 1 of a sliding block on an inclined plane (a) geometry definition of the inclined surface (b) geometry definition of the block, definition of the loads and ABAQUS meshing; (c) *SSF* computed for three friction coefficients from 3D-LEM and SSF_{FEM} from QSE-FEM; (d) sliding trajectory in XY plan of the block with ABAQUS

• *Example 2 – Column with locally large uplift pressures*

The second example is used to illustrate the effect of vertical uplift pressures locally larger than the self-weight of column B of the structure shown in Fig. 8a. Eq. (5) includes the friction force expression $F_F = (\boldsymbol{W} + \boldsymbol{U} + \boldsymbol{F} + \boldsymbol{\Delta P}).\boldsymbol{u_3} * \frac{\tan(\Phi)}{SSF}$ regardless of its sign. It is possible to obtain a

393 negative F_F value if there is a tensile normal force along $\boldsymbol{u_3}$. In this case, F_F has no physical
394 meaning. Considering a structure made of two tied columns A and B (Fig. 8a), the loads are the
395 self-weights $\boldsymbol{W_A}$ =8 kN and $\boldsymbol{W_B}$ =1 kN for A and B respectively; the uplift pressure $\boldsymbol{U}$=1 kPa and
396 a horizontal external thrust $\boldsymbol{F}$=1 kN. The friction coefficient μ_{crack} equals 0.84 between the
397 structure and the foundation. The uplifting force locally under B (2 kN), is larger than the self-
398 weight ($\boldsymbol{W_B}$ =1 kN), making this column intuitively "floating" if considered as a free-standing
399 element, even if the complete structure A-B is stable. In that case, using independent free-body
400 diagrams for A and B, no friction can occur between column B and the foundation because there
401 should be no contact. Thus, the expression $F_F = (\boldsymbol{W + U + F + \Delta P}).\boldsymbol{u_3} * \frac{\tan(\Phi)}{SSF}$ equals 0 for
402 column B. To test whether we should neglect F_F in the case of "floating" columns, two analyses
403 were performed with 3D-LEM: The first with Eq. (5) and the second with a procedure added to
404 neglect F_F when its sign is negative. Fig. 8d illustrates the response obtained with Eq. (5) (lowest
405 curve) and the modified equation, which neglect F_F for column B (highest curve). The red point
406 in Fig. 8d represents the result computed from QSE-FEM. The correlation between the lowest
407 curve and the red point in Fig. 8d and the analytical solution, which is μ_{crit}=0.2 (μ_{crit}=$\boldsymbol{F}$(1kN) /
408 [$\boldsymbol{W_A}$(8kN) + $\boldsymbol{W_B}$ (1kN) – $\boldsymbol{U}$(4kN)] = 0.2), demonstrates that the analysis using Eq. (5) directly is
409 correct. Neglecting F_F for "floating" columns changes the quantity $\boldsymbol{\Delta P_i = P_i - P_{i-1}}.\boldsymbol{\Delta P_i}$ that
410 symbolizes the available resistive strength of the ith column. It is thus important to not modify Eq.
411 (5) because to neglect the negative value of F_F is similar to not considering "weak" columns (such
412 as column B) and overestimating SSF_{LEM}.
413

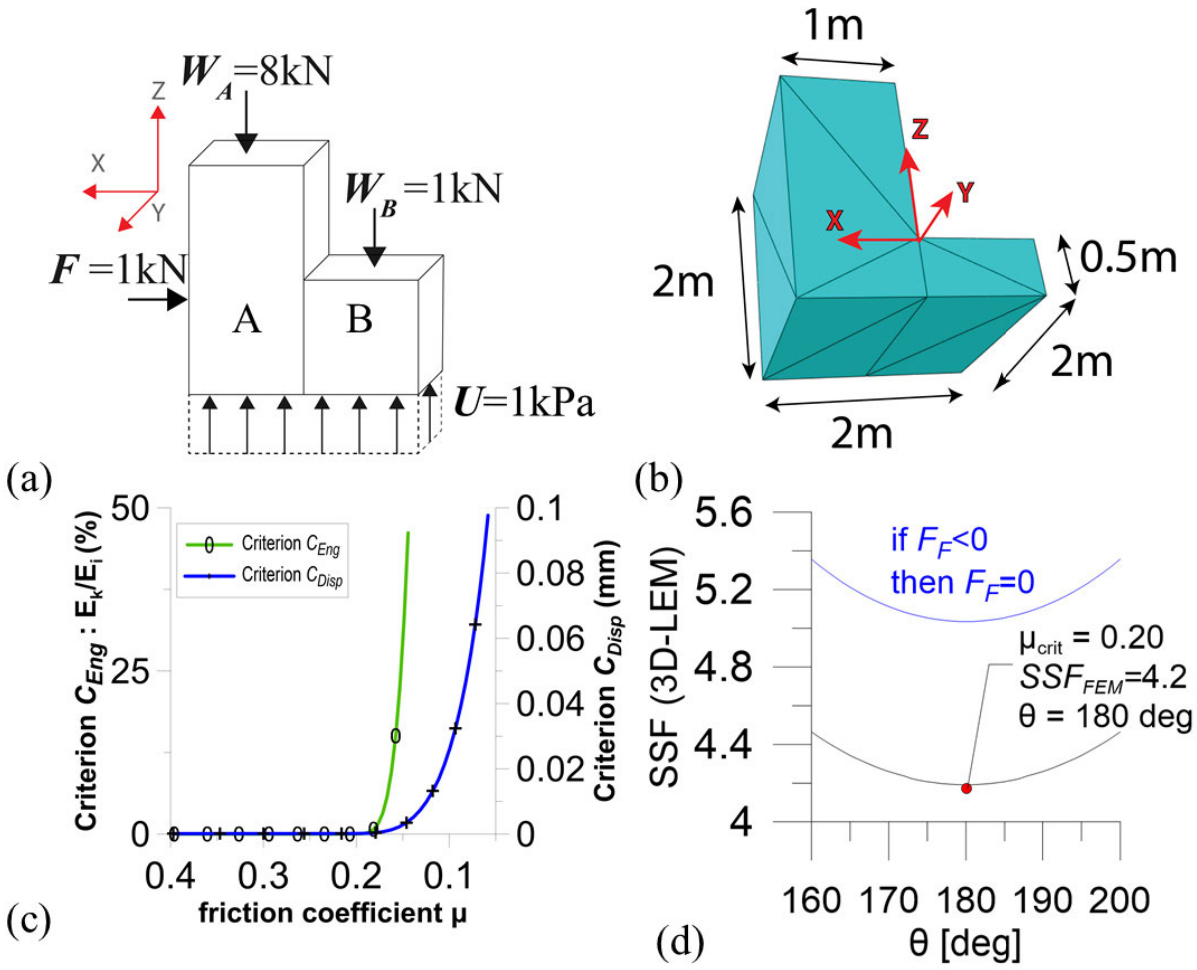

414

415 Figure 8: Example 2 with locally large uplift pressures (a) loads applied; (b) geometry of the
416 problem and ABAQUS meshing; (c) criteria of QSE-FEM; (d) *SSF*(θ) according to different
417 considerations on F_F value, and QSE-FEM result

418

419 • *Example 3- Extruded 2D gravity dam – Multi-wedge analysis*

420 The example seeks to compute the sliding safety factor (SSF_{LEM}; SSF_{FEM}) of a 2D 12 m high
421 gravity dam resting on a rock foundation (Fig. 9). This problem has been solved, with detailed
422 calculations, by the standard 2D LEM using a multi-wedge analysis [15, 20, 21, 22]. A non-planar
423 failure surface is formed within the soil and rock foundation and along the dam-foundation

interface. The dam-foundation system is divided into 5 adjacent wedges. There are two driving soil wedges, one structural wedge, and two resisting soil wedges. The loads acting on each wedge i are the wedge weight, $\boldsymbol{W_i}$, uplift pressures $\boldsymbol{U_i}$, hydrostatic pressure $\boldsymbol{H_i}$, and vertical water weight $\boldsymbol{V_i}$. As in the original reference [20], and to be able to draw meaningful comparisons, the uplift pressures are kept constant during the strength reduction process.

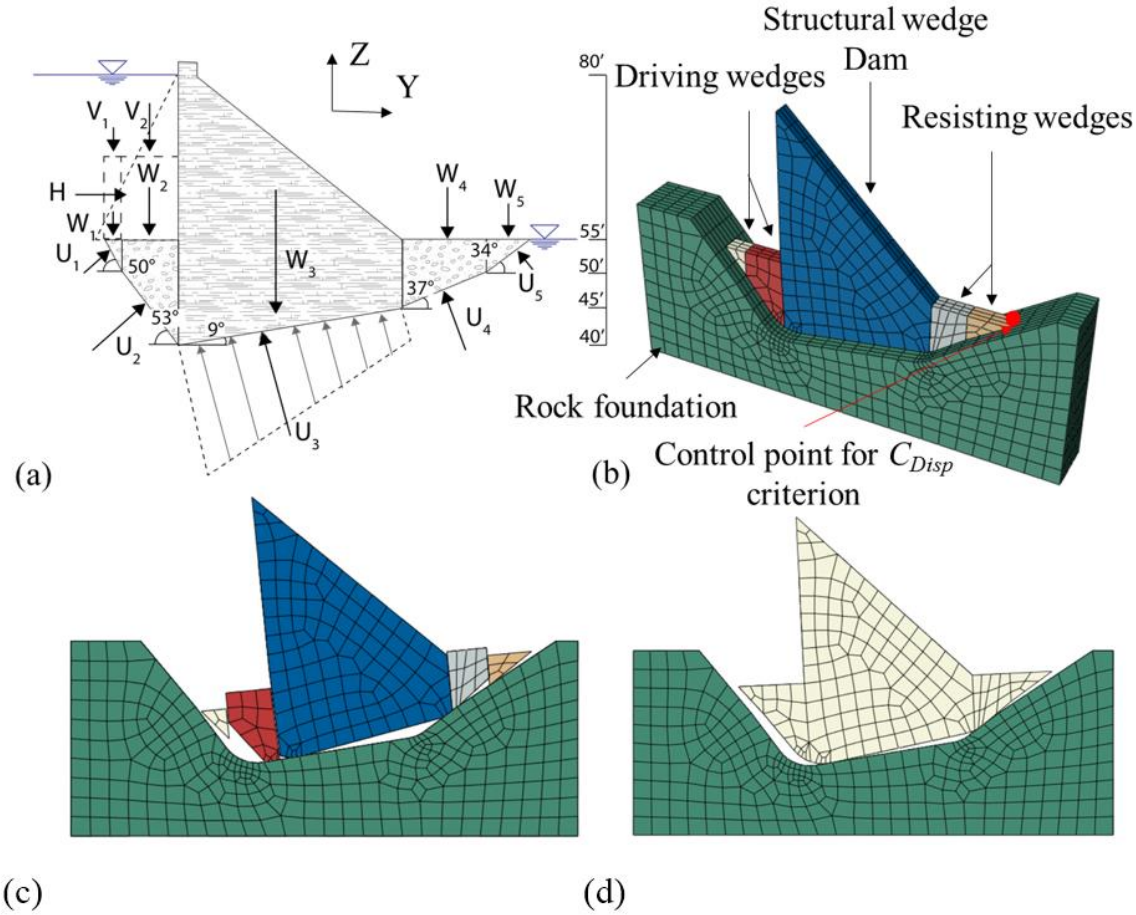

Figure 9: Example 3 of hydraulic structure presented in [20] (a) multi-wedge 2D problem; (b) ABAQUS mesh; (c) wedge displacements of the *contact* problem (scale: 10/1); (d) wedge displacements of the *tied* problem (scale: 10/1)

Despite its apparent simplicity, this problem is particularly challenging due to the following issues: (1) The presence of sharp contact edges at the intersection of the wedges and sensitivity of the General contact algorithm to this condition; (2) The effect of shear and moment transfer along the vertical interfaces between the wedges; (3) The driving force in the problem that is the hydrostatic force ***H*** acting on the upstream face of the dam or wedge 3. This force is exerted on the third wedge element (and not the first) in the wedge chain and results in tensile stresses between the second and third wedges and an overturning tendency of the dam. (4) The abutment effect developed due to resisting soil wedges.

Clearly, most of these issues are outside the 3D-LEM tool application range. QSE-FEM can be used to study each issue separately, but this is also outside the scope of this paper. The effect of sharp contact edges has been studied, and no significant effect was found in SSF_{FEM} or in the final instability mechanism. The effect of vertical interfaces between wedges was tested using two conditions: a contact condition with no friction and a full compatibility (or tied) condition. The results of the QSE-FEM are dependent on these conditions and are listed in Table 1 by QSE-FEM-contact and QSE-FEM-tied for *contact* and *tied* conditions, respectively.

Table 1: Example 3: Extruded 2D Gravity Dam

USACE 2005	3D-LEM	QSE-FEM-contact	QSE-FEM-tied
SSF_{LEM}	SSF_{LEM}	SSF_{FEM}	SSF_{FEM}
2.0	1.96	2.1	> 8.0

One of the advantages of the explicit solution tool in ABAQUS compared to the standard implicit resolution is the way contacts on interfaces are managed, especially how contact between two coincident nodes from a wedge and the foundation is modelled. In the standard implicit tool, the tangential contact before sliding is represented by a penalty coefficient. This allows displacements named “elastic slip”, even if the shear stress is below the allowable frictional shear strength described by Mohr–Coulomb equation. Another alternative for the implicit solution (ABAQUS-Standard) is to use the Lagrange multiplier method to enforce exactly the kinematic tangential sticking constraints of the potentially sliding interfaces. This solution tends however to increase the complexity of the problem and convergence issues may arise ([9]). Fig. 10 represents several displacement responses in the *tied* conditions for constant friction coefficients reduced by a factor of 2 from the initial values. In the implicit analyses, the tangential penalty coefficient is increased systematically to study convergence properties. The implicit solutions are converging to the explicit solution while the penalty coefficient is increasing. QSE-FEM uses the equivalent of an infinite tangential penalty coefficient, which reduces the “elastic slip” to zero. This makes the explicit solution much more efficient than the standard implicit one to detect sliding motions.

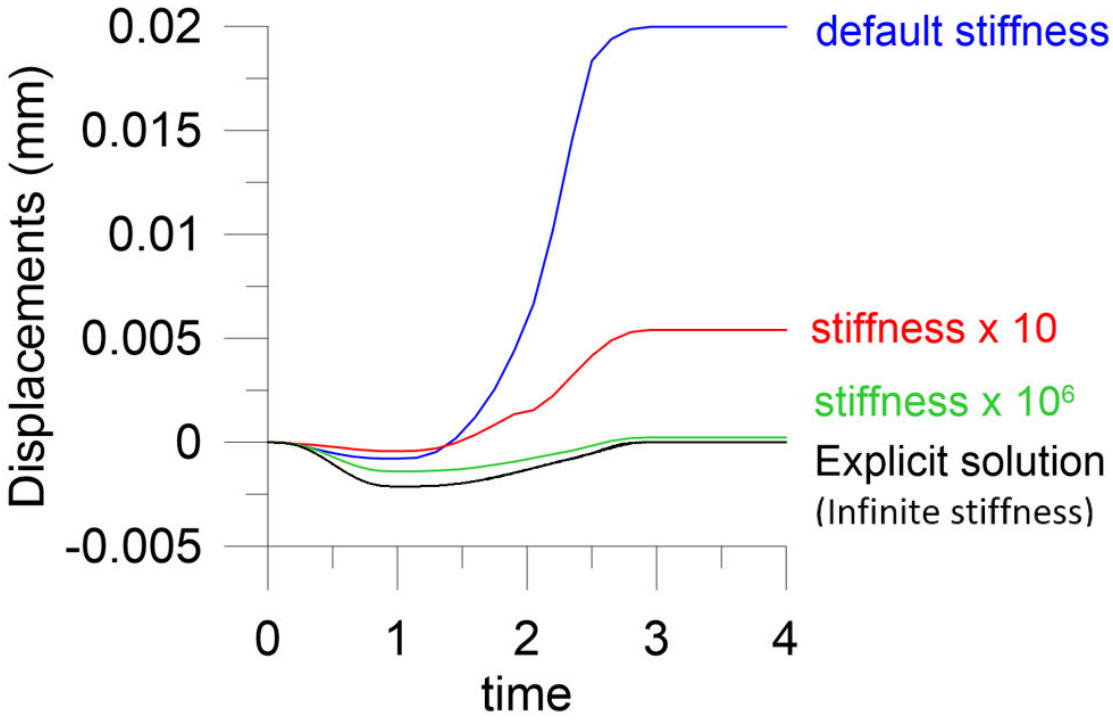

Figure 10: Absolute displacements of the control point. Convergence of the standard implicit solutions towards the explicit solution when stiffness is increasing. Computed on tied example 3 *SSF=2*

A good correlation is found for *SSF*, between [20], 3D-LEM and QSE-FEM-contact conditions. QSE-FEM-tied resulted in a large value of SSF_{FEM}, which can be attributed to the abutment effect of resisting soil wedges. Fig. 11 presents the evolution of the computed SSF_{FEM} versus the horizontal displacement of the control point. A similar tendency has been reported by Wei et al. [23] and demonstrates the obvious dependency of *SSF* on the displacement of the control point (equal to sliding for infinitely rigid blocks). The problem therefore becomes an *engineering problem* to decide on the threshold displacement (or sliding) value and compute the corresponding *SSF* according to Fig. 11.

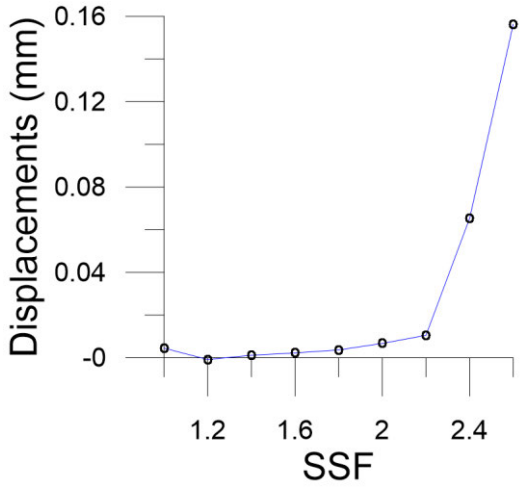

Figure 11: Horizontal displacements of the control point for untied example 3

6 Spillway analysed

This section presents the sliding stability analysis of a concrete hydraulic structure adapted from an existing spillway suffering from AAR as shown in Fig. 1.

6.1 Description

The AAR swelling displacements induced severe cracking at the base end of the gravity dam and the spillway pier adjacent to it (Fig. 1b). The crack and the top of the hydraulic structure separate the extremities of the concrete block. Water flow is visible on the downstream face of the gravity dam (Fig. 1c). The crack is thus going from the upstream to the downstream face. The upper block is considered independent of the rest of the structure and is free to move in any direction. In the existing structure, passive steel anchors have been added to improve the sliding safety. These anchors have not been considered in this application.

The material and crack interface properties of this block are displayed in Table 2. Four load conditions are considered: the weight due to gravity (G), the horizontal hydrostatic pressure (H),

499 the horizontal gate thrust (V) on the left of the pier and the uplift pressures (U). Thus, we define
500 one load combination including all load conditions: GHVU. In the context of this application
501 example, we exclude any consideration of AAR effects.
502
503 Table 2: Material Properties

Material properties		
ρ (kg/m^3)	Density	2 400
E (MPa)	Young modulus	25 000
ν	Poisson coefficient	0.2
μ_{crack}	Friction coefficient	1.13
C (kN/m^2)	cohesion	0.0

504
505 The hydrostatic loads and uplift pressures are defined according to the following outlines: (1) the
506 hydrostatic pressure is maximal upstream of the gate and (2) it linearly decreases downstream of
507 the gate until reaching atmospheric pressure at the downstream face of the gravity dam (Fig. 12).
508 The maximal pressure is defined as the water column height from the crest of the pier and the dam.
509 For simplicity, the uplift pressure diagram was kept constant during the strength reduction process.
510 The gate thrust is produced by the horizontal hydrostatic pressure acting on the gate adjacent to
511 the pier. The gate is 15 m long, and the half-force resultant of this pressure is transmitted to the
512 pier.
513

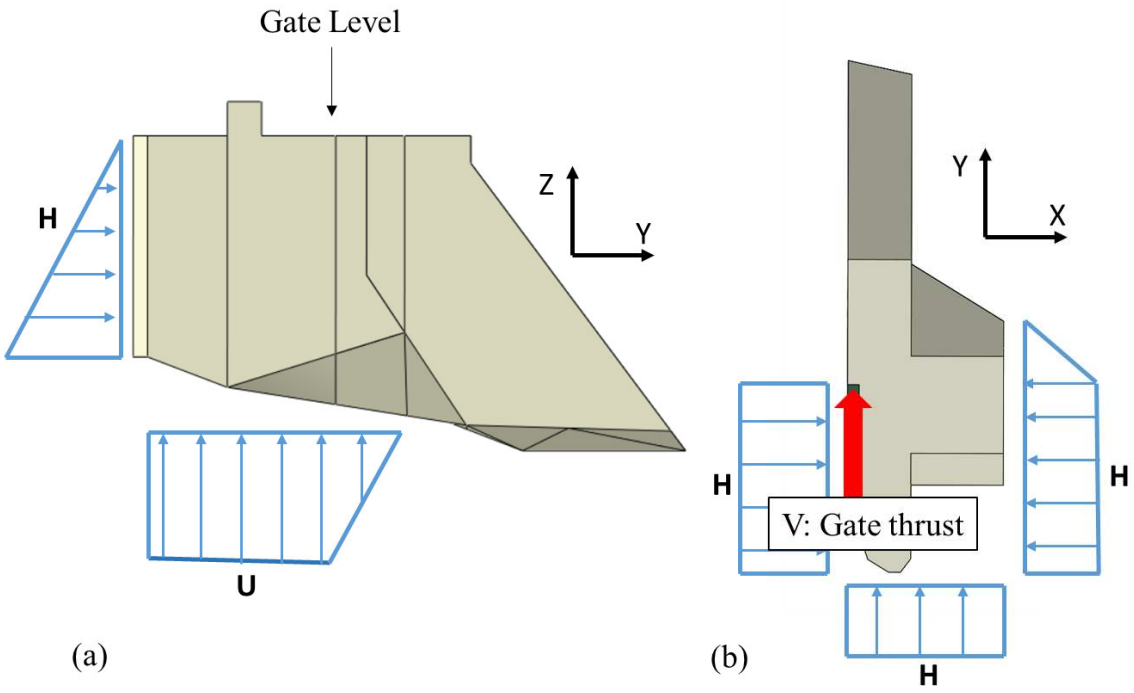

Figure 12: Load conditions on the concrete wedge: H Hydrostatic pressure, U Uplift and V Gate thrust : (a) elevation view; (b) plan view

6.2 Stability assessment

The friction coefficient of the concrete/concrete cracked interface is $\mu_{crack} = 1.13$. Table 3 displays SSF_{LEM} and SSF_{FEM} and the related sliding directions $\boldsymbol{D}$ for the load combination GHVU.

Table 3: Comparative results for the GHVU load combination

3D-LEM		QSE-FEM		
SSF_{LEM}	$\boldsymbol{D_{LEM}}$ θ (deg)	SSF_{FEM} Criterion C_{Eng}	SSF_{FEM} Criterion C_{Disp}	$\boldsymbol{D_{FEM}}$ θ (deg)
1.66	106	1.94	1.78	105

In the load combination GHVU, SSF_{LEM} = 1.66 is the lower bound in regard to SSF_{FEM} computed with the criteria C_{Eng} (SSF_{FEM} = 1.94) and C_{Disp} (SSF_{FEM} = 1.78). The sliding direction θ_{LEM} = 106 deg is very close to θ_{FEM} = 105 deg.

The ABAQUS mesh is used for QSE-FEM analyses, and the two convergence criteria for a friction coefficient interval range of [1.13; 0.2] are shown in Fig. 13. According to Fig. 13b, μ_{crit}, the critical friction coefficient inducing sliding, lies between 0.7 and 0.4. The methodology described in section 4 was thus applied to reduce uncertainty on μ_{crit}. The main observations led to steps a) to g) as follows. Step a: the crack surface geometry was modelled in ABAQUS only according to the onsite measurement of the crack rim, so uncertainty remains in the exact crack surface geometry. Linear tetrahedral FEs were used. Different mesh sizes were tested during the analyses, and no significant influence on SSF_{FEM} or SSF_{LEM} was found. Step d: based on θ_{LEM} = 106 deg computed in step c, the monitoring node was defined as shown in Fig. 13a. SSF_{FEM} equals 1.66, corresponding to μ_{LEM} = 0.683. Thus, the initial value of the friction coefficient for QSE-FEM was set up to μ_0=0.7. Step e: the first interval range computed for μ_{crit} was $[\mu(t_{low}) = 0.7, \mu(t_{up}) = 0.45]$. The two verification analyses were performed with $\epsilon = 5\%$ and validated the interval range. Another analysis with the reduced interval range $[\mu(t_{low}) = 0.65, \mu(t_{up}) = 0.5]$ was then performed, and two new verification analyses ($\epsilon = 5\%$) validated the new interval. Step g: using the two criteria C_{Disp} and C_{Eng}, the friction coefficients were found: $\mu_{crit}(C_{Disp}) = 0.637$ and $\mu_{crit}(C_{Eng}) = 0.585$. The corresponding $SSF_{FEM} = \frac{\mu_{crack}}{\mu_{crit}}$ values are shown in Table 3.

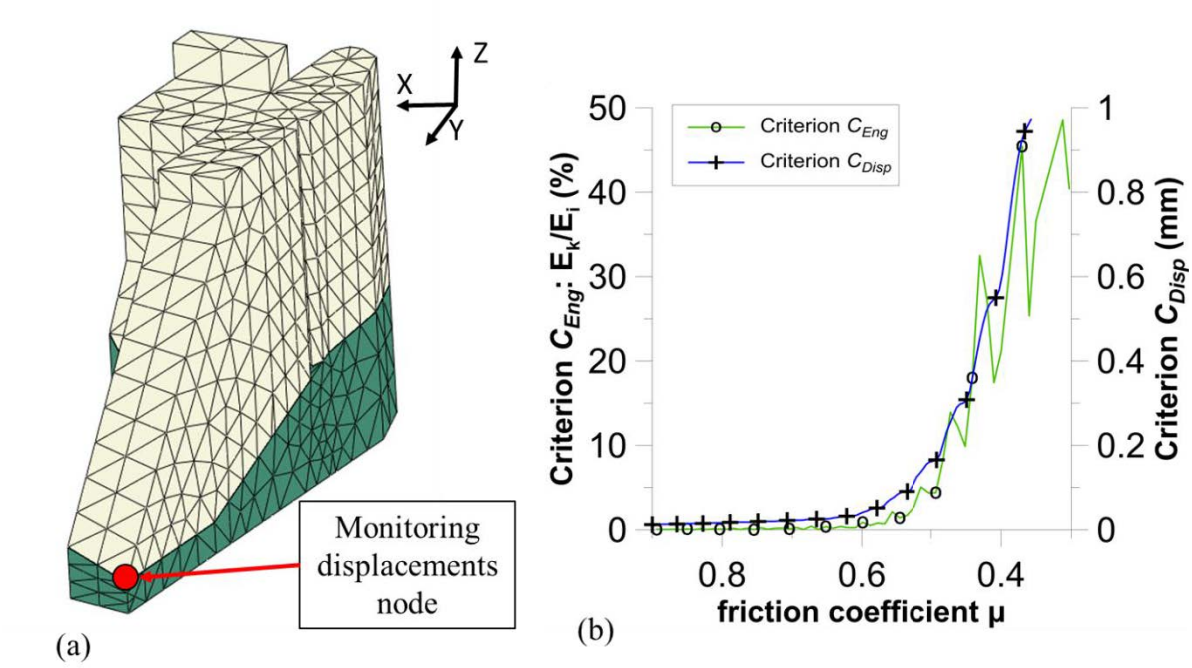

Figure 13: Quasi-static explicit FE method (QSE-FEM) analysis with ABAQUS; (a) the monitoring displacements node is selected according to the sliding kinematic motion; (b) C_{Eng} and C_{Disp} criteria response for the GHVU load combination

7 Conclusions

A methodology to study the sliding safety of hydraulic structures with an a priori known 3D discrete cracked surface geometry has been presented. This methodology is based on two complementary tools using a shear strength reduction method: (1) the Quasi-Static Explicit Finite Element Method (QSE-FEM) exhibiting robust convergence properties for highly nonlinear problems and (2) the tridimensional limit equilibrium method (3D-LEM). 3D-LEM developed in this work is an extension of the classical 2D limit equilibrium [20] considering force equilibrium in the sliding direction but neglecting moment equilibrium. 3D-LEM computes sliding safety factors (*SSF*) along any potential sliding direction ***D*** for arbitrary cracked surface geometry. Three benchmark examples were studied to verify and validate the proposed methodology. A case study,

adapted from an existing cracked hydraulic structure, was then presented. Though applied on an example of hydraulic structure, the framework developed in this study can be applied to a wider range of civil engineering problems where failure may occur through complex and arbitrary 3D surface.

The following conclusions were drawn while developing and applying the proposed methodology:

1. The 3D-LEM tool is simple to implement and to interpret in regards to tridimensional QSE-FEM analyses, which require significant resources and expertise. 3D-LEM should be used in complement to QSE-FEM to estimate the critical friction coefficient and sliding direction, $\boldsymbol{D_{FEM}}$. Strong correlation was found for *SSF* and sliding direction $\boldsymbol{D}$ between QSE-FEM and 3D-LEM for pure translational kinematic motion problems without any rotation (crack opening). For more complex problems, such as the hydraulic cracked structure (Fig. 1), 3D-LEM was found to be a lower bound to estimate μ_{crit} and related SSF_{LEM} in regard to QSE-FEM, SSF_{FEM}.

2. One major difficulty with explicit finite element analyses is to identify sliding initiation. A criterion based on the ratio of kinetic energy to internal strain energy has been shown to be insufficient. A new criterion based on absolute displacements of a control point, located at the extremity of the sliding crack surface, was found to be effective to detect incipient sliding failure.

3. While using the strength reduction method, it was shown that the friction coefficient μ must be reduced in a series of "smooth steps" including two stages: (1) cubic polynomial

decrease of $\mu(t)$; (2) nearly constant value of $\mu(t)$. This procedure allows accurate monitoring of the control point displacements and determination of the critical friction coefficient μ_{crit} to initiate sliding motions.

4. Ill conditioning is possible in 3D-LEM for complex geometries. Because the exact crack surface geometry remains uncertain in most cases, the geometry is locally adjusted in 3D-LEM to ensure convergence [15].

5. The third benchmark example (multiple wedges problem [20]) revealed to be a challenging problem to solve with QSE-FEM. The geometry of the cracked surfaces with sharp concave angles, and the importance of the overturning moment induced by the applied loads favour a rotational motion in addition to sliding, which could not be accounted for in 3D-LEM. Two versions of this problem were studied: the contact and untied problems. The untied problem gave results close to the limit equilibrium method (LEM) and to 3D-LEM. The tied problem requires more studies, which are outside the scope of this paper.

Following this research work, some further developments are underway:

1. Structural modelling using QSE-FEM has been undertaken to consider a highly nonlinear concrete material constitutive model, including strength and stiffness degradation due to alkali–aggregate reaction. QSE-FEM is expected to allow modelling, in a robust way, of hydraulic structures with complex multi-crack patterns.
2. The modelling of the effect of rehabilitation work using passive or post-tensioned steel anchor bars has been initiated.

Acknowledgements

The financial support provided by the Quebec Fund for Research on Nature and Technology and the Natural Science and Engineering Research Council of Canada is acknowledged. The authors would also like to thank Hydro-Quebec Engineers for their fruitful collaboration and discussions.

References

[1] Huang, M., & Pietruszczak, S. (1999). Modeling of thermomechanical effects of alkali-silica reaction, *ASCE Journal of Engineering Mechanics*, Vol.125, No.4 pp. 476- 485.

[2] Comi, C., Fedele, R., & Perego, U. (2009). A chemo-thermo-damage model for the analysis of concrete dams affected by alkali-silica reaction, *Mechanics of Materials,* Vol. 41, pp. 210-230.

[3] Bérubé, M.-A., Durand, B., Vézina, D., & Fournier, B. (2000). Alkali-aggregate reactivity in Québec (Canada), *Canadian Journal of Civil Engineering*, Vol. 27, pp. 226-245.

[4] Goguel, B., Arch Dam case studies, (2009). Symposium on Alkali Aggregate reactions in Concrete Dams, Paris, France, September, 15.

[5] Sellier, A., Bourdarot, E., Multon, S., Cyr, M., and Grimal, E. (2009). Combination of Structural Monitoring and Laboratory Tests for Assessment of Alkali-Aggregate Reaction Swelling: Application to Gate Structure Dam, *ACI Materials Journal*, Vol. 106, No. 3, pp. 281-290.

627

628 [6] Bourdarot, E., Sellier, A., Multon, S., & Grimal, E. (2010). A review of continuum damage
629 modelling for dam analysis, *European Journal of Environmental and Civil Engineering*, Vol. 14,
630 No. 6-7, pp. 805-822, DOI: 10.1080/19648189.2010.9693263.

631

632 [7] Tu, Y., Liu, X., Zhong, Z., & Li, Y. (2016). New criteria for defining slope failure using the
633 strength reduction method, *Engineering geology*, Vol. 212, pp. 63-71, DOI:
634 10.1016/j.enggeo.2016.08.002.

635

636 [8] Ben Ftima, M. (2013). Using nonlinear finite element methods for the design of reinforced
637 concrete structures : application to massive structures, Ph.D thesis (in French), École
638 Polytechnique de Montréal, Montréal, Canada.

639

640 [9] Hibbitt, H. D., Karlson, B. I. & Sorensen, E. P. (2014). ABAQUS version 6.14, *finite element*
641 *program*, Hibbitt, Karlson and Sorensen, Providence, R.I.

642

643 [10] Lemos J. V. (2008). Block modelling of rock masses, European Journal of Environmental
644 and Civil Engineering, Vol.12, No.7-8, pp. 915-949

645

646 [11] Lisjak, A., & Grasselli, G. (2014). A review of discrete modeling techniques for fracturing
647 processes in discontinuous rock masses. Journal of Rock Mechanics and Geotechnical Engineering
648 Vol.6, pp. 301-314.

649

[12] Zhou, W., Yuan, W., Ma, G. & Chang, X-L. (2016). Combined finite-discrete element method modeling of rockslides. Engineering Computations, Vol. 33, No. 5, pp.1530-1559.

[13] Ben Ftima, M., & Massicotte, B. (2015). Utilization of nonlinear finite elements for the design and assessment of large concrete structures, part II: Applications, *ASCE Journal of Structural Engineering*, Vol. 141, No. 9, DOI: 10.1061/(ASCE)ST.1943-541X.0001178.

[14] Ben Ftima, M., Sadouki, H., & Brühwiler, E. (2016). Development of a computational framework for the use of nonlinear explicit approach in the assessment of concrete structures affected by alkali-aggregate reaction, Proceedings, 9th International Conference on Fracture Mechanics of Concrete and Concrete Structures, FRAMCOS-9, V. Saouma, J. Bolander, and E. Landis (Eds), May 22-25, Berkeley, California, USA, 11 pp.

[15] Ebeling, R.M., Fong, M.T, Wibowo, J.L., & Chase, A. (2012). Fragility Analysis of a Concrete Gravity Dam Embedded in Rock and Its System Response Curve Computed by the Analytical *Program GDLAD_Foundation*, US Army Corps of Engineers, Engineer Research and Development Center, Report No. ERDC TR-12-4, Pittsburgh, PA, USA.

[16] Prior, A. M., (1994). Applications of implicit and explicit finite element techniques to metal forming, *Journal of Materials Processing Technology*, Vol. 45, No. 4, pp. 649-656.

[17] Hallquist, J.O., (2006). LS-DYNA: Theory manual, Livermore Software Technology Corporation (LSTC), CA, USA.

673

674 [18] Gholami, T., Lescheticky, J., & Paßmann, R. (2003). Crashworthiness Simulation of
675 Automobiles with ABAQUS/Explicit, *ABAQUS User' Conference*, Munich, Germany, 18 pp.

676

677 [19] Fronteddu, L., Léger, P., & Tinawi, R. (1998). Static and Dynamic Behaviour of Concrete
678 Lift Joints Interfaces, ASCE Journal of Structural Engineering, Vol.124, No.12, pp.1418-1430.

679

680 [20] US Army Corps of Engineers (USACE) (1981). Sliding stability for concrete structures,
681 Engineering Technical Letter No. ETL 1110-2-256, Washington, D.C., USA.

682

683 [21] US Army Corps of Engineers (USACE) (1995). Engineering and design, gravity dams,
684 Report No EM 1110-2-2200 1995, Washington, D.C., USA.

685

686 [22] US Army Corps of Engineer (USACE) (2005). Stability Analysis of Concrete Structures,
687 Engineering and Design, Report No EM 1110-2-2100 2005, Washington, D.C., USA.

688

689 [23] Wei, W.B., Cheng, Y.M., & Li, L. (2009). Three-dimensional slope failure analysis by the
690 strength reduction and limit equilibrium methods, Computers and Geotechnics Vol. 36, pp. 70–80.

691